Vascular Tree Construction with Anatomical Realism for Retinal Images

Kai-Shung Lin[1] Chia-Ling Tsai[2] Michal Sofka[3]
Chih-Hsiangng Tsai[1] Shih-Jen Chen[4] Wei-Yang Lin[1]
[1]National Chung Cheng University
Chiayi 621, Taiwan
[2]Iona College
New Rochelle, NY 10801, U.S.A.
[3]Siemens Corporate Research
Boston, MA U.S.A.
[4] Taipei Veterans General Hospital,
Taipei 11217, Taiwan

Abstract

In this paper, we present a method to automatically extract the vessel segments and construct the vascular tree with anatomical realism from a color retinal image. The significance of the work is to assist in clinical studies of diagnosis of cardio-vascular diseases, such as hypertension, which manifest abnormalities in either venous and/or arterial vascular systems. To maximize the completeness of vessel extraction, we introduce vessel connectiveness measure to improve on an existing algorithm which applies multiscale matched filtering and vessel likelihood measure. Vessel segments are grouped using extended Kalman filter to take into consideration continuities in curvature, width, and color changes at the bifurcation or crossover point. The algorithm is tested on five images from the DRIVE database, a mixture of normal and pathological images, and the results are compared with the groundtruth images provided by a physician. The preliminary results show that our method reaches an average success rate of 92.1%.

1. Introduction

Realization of the high-level organization of the vascular trees plays an important role in a variety of medical diagnosis. It provides valuable information for the physicians to perform surgical planning and outcome assessment, and to monitor the progression of vascular diseases [23]. In cardiology, with the complete map of the vascular trees, the neurosurgeons and radiologists can make the best decision about vessel occlusion for stroke prevention that ensure collateral flow provided by other parts of the circulation [18]. In ophthalmology, measurements specific to the arterial vascular trees can provide early diagnosis of certain cardiavascular diseases. Clinical studies suggest that narrowing of the arterial blood vessels in the retina may be an early indicator of hypertension [26], [3] and atherosclerosis, which is a process of inflammation in the vessel wall leading to plaque formation and a reduction in arterial flexibility [10]. To quantify the severity of arteiolar narrowing, measurements can be drawn by comparing morphological characteristics of the arterial trees to the venous trees by measuring the changes of the arteriolar-to-venular diameter ratio, changes of the branching angles, and reduction of microvascular densities [11], [20], [25]. In terms of retinal image analysis, important features, such as the optic disk and macula, can be automatically located using the vascular trees. This is crucial for diagnosis of diseases such as macular degeneration—drusens close to the macular need immediate attention, whereas drusens on the periphery might need to be monitored only. Thus, a reliable method for vascular tree construction and quantification would be beneficial in medical diagnoses.

There is a rich body of literature on extraction of tubular structures in medical images, but the focus has mostly been on identification of vessel pixels [9], [12], [15], and segmentation of vessel segments [1], [17], [22], not delineation of the vascular network as a whole with a tree structure. Two major approaches for construction of vascular trees can be found in the literature. One approach is to grow either the vascular regions, which are later transformed into vascular trees [21], [27], or the skeletons directly [8], [16], starting from some seed points. The other approach is to build the trees from detected vessel segments using techniques of perceptual grouping [2], [4], [5], [6], [13]. We refer to the former as "growing-based" method and the latter as "grouping-based" method.

For growing-based methods, Selle et al. [21] segment vessels using a threshold-based region-growing method, with the threshold value automatically generated. The segmented vascular structure is skeletonized, and transformed into a vascular "forest", which contains a number of directed acyclic graphs, using a graph theoretical method. A similar approach is done by Yim et al. [27]. The tree is generated by Ordered Region Growing (ORG) technique. A seed is provided at the root of the tree. The growth, started from a user-defined point, is in the direction of higher intensity. The result of ORG is a graph. However, it is not clear how the ramifications are handled. Following ORG is either skeletonization or pruning. Instead of extracting the vascular regions, Haris et al. [8] and Liu et al. [16] perform tracing of the vessel centerlines. In [8], [16], the tree is

978-0-7695-3656-9/09 $25.00 © 2009 IEEE
DOI 10.1109/BIBE.2009.18

constructed as the vessels are being traced. Starting from a seed point, vessel pixels are found recursively along the vessel centerline. Ramifications are handled in a breadth-first-search manner.

For grouping-based methods, Jomier et al. [13] and Bullitt et al. [2] both perform grouping of vessel segments to form a minimum spanning tree, but with different minimization criteria. [13] minimizes the Mahalanobis distance of features defined at each junction, while [2] performs the minimization based on linear distance and image intensity in suspected regions of connection. Coppini et al. [4] propose a bottom-up coronary artery extraction method based on the angiogram edges. These edges are grouped into edge segments, which are organized to bar primitives and, finally, bars are linked to form artery segments. The algorithm developed by Deschamps et al. [5], [6] first converts the vascular image to a threshold "vessel potential" image and perform perceptual grouping and contour completion. Contours are found as minimal paths between connected components, using the fast marching algorithm.

A common problem with aforementioned works in the literature is lack of anatomical realism that reflects the true topologies of the vascular trees. In retinal images vessels are organized in trees with roots inside the optic disc. This is the region where arteries and veins enter the retinal surface. Following the main arteries and veins, vessels branch out until capillaries (the thinnest retinal vessels) are reached. However, vascular tree construction from retinal images poses several challenges:

1) Some vessels are partially traced and the traced segments are not attached to the segment of the vessel from which it branches out. Such segments are often found near the optic disk.
2) A vessel with central reflex can be mistaken as two parallel vessels. Such a vessel is brighter in the center and darker at the boundaries, appearing as a hollow vessel. The opposite occurs as well—two nearby parallel vessels being treated as one vessel.
3) A vessel is incorrectly placed between two pathological structures of higher intensity.
4) Crossovers are turned into branching points, due to incomplete tracing of some vessels.

In this paper, we present a method that improves on an existing vessel segmentation algorithm proposed by Sofka et al. [22] for retinal images and performs grouping on the extracted vessel segments to achieve anatomical realism of the vascular trees. This allows quantification of geometrical and topological properties of veins and arteries. For vessel segmentation, both vesselness and connectiveness are exploited to maximize the completeness of extraction of vessel segments. For grouping, Kalman filter is adopted to ensure continuity of vessel segments at the bifurcation or crossover point by taking into account the variations in width, curvature, and intensity along the current segment. The algorithm is tested and validated using a subset of images from the DRIVE dataset.

2. Vessel Segmentation

Our vessel extraction algorithm improves upon the algorithm by sofka [22], which determines the vesselness of a pixel based on a likelihood ratio test that combines matched filter responses, confidence measures and vessel boundary measures. Matched filter responses are derived in scale-space to extract vessels of widely varying widths. A vessel confidence measure is defined as a projection of a vector formed from a normalized pixel neighborhood onto a normalized ideal vessel profile. Vessel boundary measures and associated confidences are computed at potential vessel boundaries. Combined, these responses form a 6-dimensional measurement vector at each pixel. A learning technique is applied to map this vector to a likelihood ratio that measures the likelihood ratio vesselness (LRV) at each pixel.

Potential problems with LRV tracing include missing seed points for small vessels and determination of the threshold value in pruning. To mitigate both problems, we made few enhancements to LRV tracing to include detection of junction points for placement of extra seed points and combination of vesselness and connectiveness for pruning to alleviate the dependence of a single threshold value on LRV. Both enhancements are implemented using the technique of tensor voting [7] to determine whether a pixel is likely to be on a junction or a curve.

When tensor voting is performed, each pixel sends its tensor to its neighbor pixels through its voting field. The result of voting at each pixel is a variance-covariance matrix which is decomposed into the eigenvalues and eigenvectors. Let λ_{min} and λ_{max} be the minimum and maximum eigenvalues, respectively. A pixel is on a curve structure if its λ_{max} is substantially larger than λ_{min}, whereas a pixel is on a junction of two or more curves if both eigenvalues are similar. In other words, λ_{max} provides a good indication that a pixel is on a continuous structure, such as a curve, and serves as a measure of connectiveness of the pixel with its neighboring pixels, whereas λ_{min} provides the saliency for junctions. Both connectiveness and junction saliency maps are obtained from the LRV image, instead of the original image, since the former excludes non-vessel structures with well-defined boundaries, such as the optic disk.

To maximize the likelihood that at least a seed point is found on every vessel, we include both the seed points defined by the LRV tracer and also points near vessel junctions as tracing progresses. The motivation to adopt the latter is rather intuitive, since blood vessels are naturally connected and if the parent vessel has been traced, the vessels that branch out of it are less likely to be missed if

seeds are placed near the junctions. To enable identification of a junction before all vessels that come to meet are extracted, we detect potential junction locations using the junction saliency map.

Trade-off has to be made between false positive and false negative rates if pruning of the over-traced result uses only a single threshold value on the LRV. Reducing the threshold value increases both the true and false positives. To improve the robustness of pruning, we consider both vesselness and connectiveness measures of a pixel—points with high connectiveness are likely to be on a continuous structure, such as a vessel, even if the vesselness measure falls below the threshold value. Given traces produced by the matched filter, trace points of each trace are re-visited consecutively, and the vesselness and connectiveness measures are examined. If the former is below the threshold, the pixel, as well as the remaining ones in the trace, is discarded if (1) it is one of the first 3 trace points, (2) previous 2 trace points have low vesselness measures, or (3) the connectiveness is below a threshold, determined adaptively for each image.

At a crossover, it is possible that the vessel tracer follows a vessel which is not anatomically connected to its current one. As a result, the extracted vessel segment may contain segments from different blood vessels when tracing terminates. Before grouping of the vessel segments for vessel tree construction, every vessel segment is broken up into shorter pieces at junctions with other vessel segments to ensure that the basic components for grouping are segments that each contains only points from the same blood vessel.

3. Vessel Grouping

Taking the set of vessel segments from the segmentation algorithm, the grouping algorithm connects the segments to restore the topology of a vascular tree that bears anatomical realism. Figure 1 presents the overview of the grouping algorithm. The segments are dynamically ranked so that a segment of the highest priority category can be chosen to initiate the grouping process of a vessel. Ungrouped segments which intersect with the boundary of the optic disc (chosen manually) are assigned the first priority, and the set of segments each being part of a bifurcation and close to a vessel already grouped (being part of a constructed tree already) is assigned the second priority. To connect the segments to form a vessel, the process starts from an ungrouped segment with the highest priority, and iterates two steps: (1) iteratively correcting and learning the continuity pattern of the current segment using the extended Kalman filter and (2) picking the next segment with the highest continuity in the neighborhood of the end point of the current segment. If the next segment cannot be located, the process terminates for the current vessel, and the priorities of the remaining ungrouped segments are updated. The tree construction process terminates when no segment of first

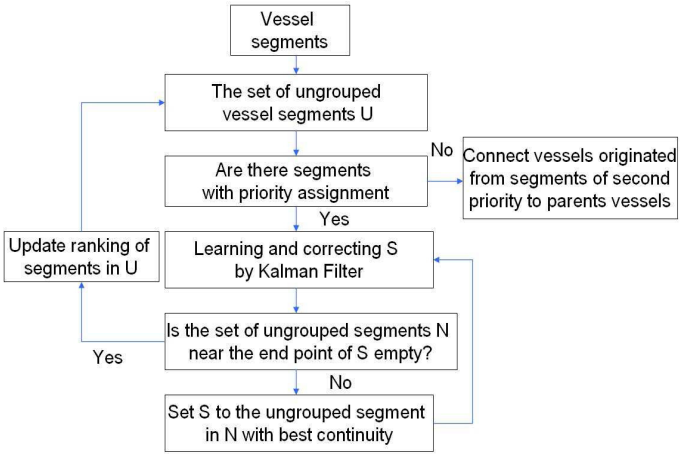

Figure 1. The flow chart of perceptual grouping process.

or second priority can be found. Constructed vessels that originate from bifurcation points are each connected to the vessel that it branches out to form a vessel tree, and the final result is a set of trees with the root segments intersecting with the boundary of the optic disk.

3.1. Training of Extended Kalman Filter

To connect two segments of a vessel, three continuity properties are imposed along a vessel: (a) the vessel direction varies constantly, (b) the lumen width varies constantly, (c) and the color intensity varies relatively constantly. An extended Kalman Filter is adopted to learn the characteristics of a vessel segment to ensure best continuity when choosing for the next segment for grouping. Each trace point $\mathbf{p}_k$ is associated with a 6-tuple, state vector $\mathbf{X}_k = (x, y, G, d, \theta, \dot{g})$, where x and y form the coordinate, G is the color intensity, d is the width, θ is the tangent direction of the vessel at $\mathbf{p}_k$, and $\dot{g}$ is the change in the color intensity. At $\mathbf{p}_k$, the nonlinear system model function and the observation function are defined as

$$\mathbf{X}_k = f_{k-1}(\mathbf{X}_{k-1}) + \mathbf{w}_{k-1} \quad (1)$$

$$\mathbf{X}_k^o = \mathbf{X}_k + \mathbf{v}_k \quad (2)$$

where $\mathbf{X}_{k-1}, \mathbf{X}_k$ are state vectors at $\mathbf{p}_{k-1}$ and $\mathbf{p}_k$, respectively. f_k is nonlinear functions as the following:

$$x_k = x_{k-1} + d_{k-1} \times \cos\theta_{k-1} \quad (3)$$

$$y_k = y_{k-1} + d_{k-1} \times \sin\theta_{k-1} \quad (4)$$

$$G_k = G_{k-1} + \dot{g}_{k-1} \quad (5)$$

$$d_k = d_{k-1} \quad (6)$$

$$\theta_k = \theta_{k-1} \quad (7)$$

$$\dot{g}_k = \dot{g}_{k-1} \quad (8)$$

$\mathbf{X}_k^o$ is the observation vector at p_k. In our application, $\mathbf{X}_k^o$ comes from the vessel tracer. $\mathbf{w}_k$ and $\mathbf{v}_k$ are the system noise and the observation noise, respectively. They encapsulate system errors which mainly come from the unpredictable vessel direction perturbation and the quantization error as the actual coordinates of centerline midpoint are discretized into integral number of pixels in the image.

The Kalman theory gives the equations for the optimal estimate $\hat{\mathbf{X}}_{k|k-1}$ given the statistics of the system and observation noise $\mathbf{w}_{k-1}$ from $\hat{\mathbf{X}}_{k-1|k-1}$. The prediction and correction functions are defined as

$$\hat{\mathbf{X}}_{k|k-1} = f_{k-1}(\hat{\mathbf{X}}_{k-1|k-1}) \quad (9)$$

$$\hat{\mathbf{X}}_{k|k} = \hat{\mathbf{X}}_{k|k-1} + \mathbf{K}_k \times (\mathbf{X}_k^o - \hat{\mathbf{X}}_{k|k-1}) \quad (10)$$

where the predict phase uses the previous state estimate $\hat{\mathbf{X}}_{k-1|k-1}$ to produce an estimate of the current state, $\hat{\mathbf{X}}_{k|k-1}$. In the correction phase, measurement information at the current $\mathbf{p}_k$, $\mathbf{X}_k^o$, is used to refine this prediction to arrive at a more accurate state estimate, $\hat{\mathbf{X}}_{k|k}$. The Kalman gain $\mathbf{K}_k$, covariances of the state and measurement noise are estimated directly from the data. For more details about Kalman filter, we refer the reader to the book written by Kay [14].

3.2. Grouping by Kalman Filter

As the Kalman filter reaches the end of a vessel segment, $\mathbf{X}_k^o$ is chose from the segments that come to meet at this junction, and the segment in which $\mathbf{X}_k^o$ resides is the one to be connected to the current segment. $\mathbf{X}_k^o$ is the state vector of the first trace point of the neighboring segment with the minimum Mahalanobis distance defined as:

$$d(\hat{\mathbf{X}}_{k|k-1}, \mathbf{X}_k^o) = \sqrt{(\hat{\mathbf{X}}_{k|k-1} - \mathbf{X}_k^o)\Sigma^{-1}(\hat{\mathbf{X}}_{k|k-1} - \mathbf{X}_k^o)} \quad (11)$$

where Σ is the diagonal covariance matrix of the estimated point $\hat{\mathbf{X}}$. The corrected state vector $\hat{\mathbf{X}}_{k|k}$ becomes the first state vector of the new segment. The grouping process for the current vessel terminates if no ungrouped segment is found near the end point of the current segment.

4. Experimental Analysis

The preliminary testing result is obtained from a test suite of five images, three relatively normal and two pathological, from the DRIVE database [24]. Images were acquired using a Canon CR6 nonmydriatic 3CCD camera at a 45 field-of-view and are 24-bit color at a resolution of 768×584 (the fundus occupies a circle of diameter approximately 540 pixels about 50% of the image). The results of vascular tree construction are compared with the groundtruth images provided by a physician. An example is shown in Figure 3(a). Each vascular tree originating from the optic disk is assigned a unique non-white color. An area is painted white if more than one vessel passes through it.

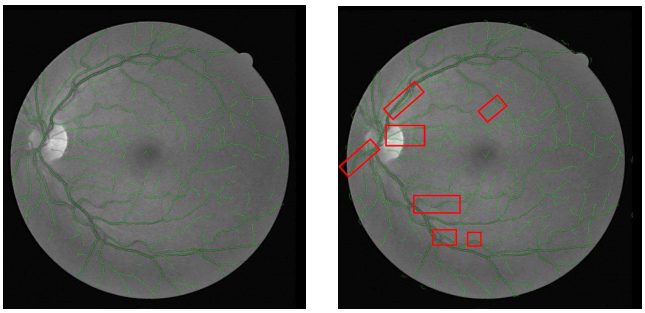

(b) (a)

Figure 2. Improvement on vessel extraction over the original LRV algorithm. (a) The result of LRV tracing with the threshold value 2.0 as set in [22]. (b) The result of our improved tracing algorithm with more seed points near vessel junctions and more robust scheme for trace point selection.

4.1. Evaluation for Vessel Extraction

Since the focus of the work is on the correctness of the tree construction, we only demonstrate qualitatively the improvement over the LRV algorithm on vessel extraction without doing a rigorous comparison using the entire DRIVE database. Figure 2(a) shows the result by the original LRV tracing, whereas Figure 2(b) is the results from our improved algorithm. The rectangles indicate vessels which are discarded by the original LRV algorithm even with the threshold value set to 1. Overall, our improved LRV tracer increases the number of traces considerably, with the majority of them being true positive. The same effect cannot be achieved by simply decreasing the threshold on the LRV value, which increases both true and false positive traces.

4.2. Evaluation for Vascular Tree Construction

To validate the correctness of the tree construction, we compare our result against the groundtruth. A segment is correctly connected to its parent segment if its color in the groundtruth image is the same as its parent segment. The success rate is defined as the percentage of correctly connected segments over the total number of segments involved in the construction process. The total number of segments does not include the false positive segments. However, if a true positive segments is connected to a false positive segment, it is treated as an incorrectly connected segment.

There is a total of 484 segments extracted. Our preliminary result shows an average success rate of 92.1% for vessel grouping (see table 1). The best case with a success rate of 95% is shown in Figure 3. The retinal image is relatively healthy with a well-defined vasculature. However, the efficacy of grouping depends heavily on the robustness of the tracing algorithm. The reason that segments shown in

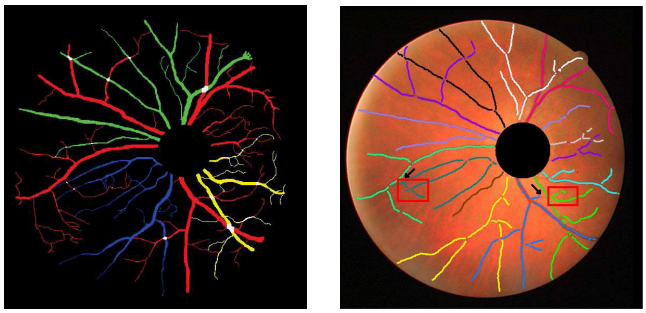

(a) (b)

Figure 3. The best case in our test suite with a success rate of 95%. (a) The vessel tree groundtruth. (b) The result of vessel tree construction. The red boxes highlight the incorrectly classified segments.

the boxes in Figure 3 are incorrectly grouped is failure in tracing, which turns a crossover to bifurcation as pointed out by the arrows. The lowest success rate is 89.8%—many segments are obtained from pathological structures, shown in Figure 4(c). In Figure 4(d), the thin yellow line is drawn manually to indicate the correct grouping if tracing were performed correctly for the thin vessel. In addition to missing vessel segments, the end section of the vessel is grouped to a false segment from a lesion (top portion of the blue line), instead of the white segment pointed to by the red arrows.

Table 1. Success rates for 5 retinal images from the DRIVE database. The overall success rate for the 5 images is 92.1% (484/446)

Image	Number of segments	Correctly connected	Success rate
No.1	120	114	95.0%
No.2	114	103	90.4%
No.4	80	76	95.0%
No.11	88	79	89.8%
No.26	82	74	90.2%

5. Discussion and Conclusion

We have presented a method which improves on an existing vessel segmentation algorithm proposed by Sofka et al. and performs grouping on the extracted vessel segments to achieve anatomical realism of the vascular trees. For vessel segmentation, both vesselness and connectiveness are exploited to maximize the completeness of vessel extraction. For vessel grouping, Kalman filter is adopted to ensure continuity of vessel segments at the bifurcation or crossover point by taking into account the variations in width, curvature, and intensity along the current segment. The main advantages are the abilities to track and measure complete vessel trees.

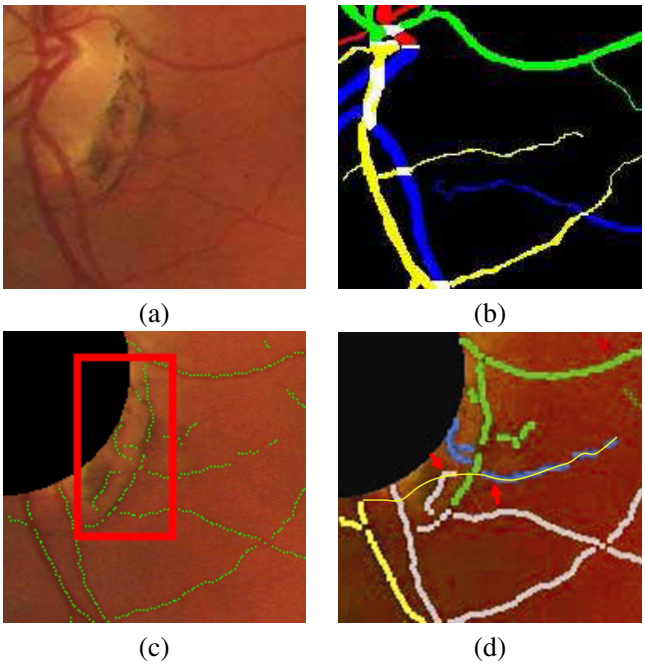

(a) (b) (c) (d)

Figure 4. The worst case in our test suite with a success rate of 89.8%. Many segments are incorrectly placed in pathological structures. (a) The original image. (b) The vessel tree groundtruth. (c) The red box highlighting the area with false positive traces. (d) The blue line is the result of incorrect grouping, whereas the thin yellow line is drawn manually to indicate the correct grouping.

The system achieves an average success rate of 92.1% in the preliminary study. With the tree type (artery/vein) provided by an operator, extracted trees allow quantification of geometrical and topological properties of veins and arteries. One such measure is the arteriolar-to-venous (A/V) ratio of the retinal vasculature, which is an important index for end-organ damage in patients with hypertension [19].

The algorithm in its present state is still prone to failure in areas where pathological structures are present (see Figure 4(c))—vessels may be connected to pathological structures. Furthermore, efficacy of grouping depends heavily on the robustness of the tracing algorithm since incorrect grouping is likely to occur at places where vessels are insufficiently traced (see Figure 3). In the next phase of development, we will focus on the correctness of grouping, instead of robustness of tracing, and improve the clinical usability of the system. The idea is to adopt a learning-based approach in which the system learns the error patterns from the physician in the validation process. With the learning capability, the confidence and prominence measures of the connections of the vessel segments can be corrected adaptive, which in turn assist the physician in the validation process so that connections with low confidence and high prominence can receive early attention.

References

[1] S. Aylward and E. Bullitt. Initialization, noise, singularities, and scale in height-ridge traversal for tubular object centerline extraction. *IEEE Trans. Med. Imaging.*, 21:61–75, 2002.

[2] E. Bullitt, S. Aylward, A. Liu, J. Stone, S. Mukherji, C. Coffey, G. Gerig, and S. Prizer. 3d graph description of the intracerebral vasculature from segmented mra and tests of accuracy by comparison with x-ray angiograms. In *Proc. IPMI*, volume 1613 of *LNCS*, pages 308–320, Visegrád, Hungary, June/July 1999. Springer-Verlag.

[3] S. Chatterjee, S. Chattopadhya, M. Hope-Ross, and P. Lip. Hypertension and the eye: Changing perspectives. *J. Hum. Hypertens.*, 16:667–675, 2002.

[4] G. Coppini, M. Demi, R. Poli, and G. Valli. An artificial vision system for x-ray images of human coronary tree. *IEEE T. Pattern Anal.*, page 156 162, Feb 1993.

[5] T. Deschamps and L. Cohen. *Geometric Methods in Bio-Medical Image Processing*, chapter Grouping connected components using minimal path techniques. Mathematics and Visualization. Springer, 2002.

[6] T. Deschamps and L. D. Cohen. Grouping connected components using minimal path techniques. application to reconstrucion of vessels in 2d and 3d images. In *Proc. CVPR*, volume 2, pages 102–109, 2001.

[7] G. Guy and G. Medioni. Interring global perceptual contours from local features. *IJCV*, 20(1):113–133, 1996.

[8] K. Haris, S. Efstratiadis, N. Maglaveras, C. Pappas, J. Gourassas, and G. Louridas. Model-based morphological segmentation and labeling of coronary angiograms. *IEEE Trans. Med. Imaging.*, 18(10):1003–1015, Oct. 1999.

[9] A. Hoover, V. Kouznetsova, and M. Goldbaum. Locating blood vessels in retinal images by piecewise threshold probing of a matched filter response. *IEEE Trans. Med. Imaging.*, 19(3):203–210, 2000.

[10] L. Hubbard, R. Brothers, W. King, L. Clegg, R. klein, L. Cooper, R. Sharrett, M. Davis, and J. Cai. Methods for evaluation of retinal microvascular abnormalities associated with hypertension/sclerosis in the atherosclerosis risk in communities study. *Ophthalmology*, 106(12):2269–2280, 1999.

[11] A. D. Hughes, E. Martinez-Perez, A.-S. Jabbar, A. Hassan, N. W. Witt, P. D. Mistry, N. Chapman, A. D. Stanton, G. Beevers, R. Pedrinelli, K. Parker, and S. Thom. Quantification of topological changes in retinal vascular architecture in essential and malignant hypertension. *J. of Hypertension*, 24(889-894), 2006.

[12] X. Jiang and D. Mojon. Adaptive local thresholding by verification-based multithreshold probing with application to vessel detection in retinal images. *IEEE T. Pattern Anal.*, 25(1):131–137, Jan. 2003.

[13] J. Jomier, V. LeDigarcher, and S. Aylward. Automatic vascular tree formation using the mahalanobis distance. In *Proc. 8th MICCAI*, page 806 812, Palm-Springs, USA, 200.

[14] S. M. Kay. *Fundamentals of Statistical Signal Processing: Detection Theory*. Prentice Hall PTR, 1998.

[15] T. Lindeberg. Edge detection and ridge detection with automatic scale selection. *IJCV*, 30:117–156, Nov. 1998.

[16] I. Liu and Y. Sun. Recursive tracking of vascular networks in angiograms based on the detection-deletion scheme. *IEEE Trans. Med. Imaging.*, 12:334 341, June 1993.

[17] V. Mahadevan, H. Narasimha-Iyer, B. Roysam, and H. Tanenbaum. Robust model-based vasculature detection in noisy biomedical images. *IEEE Trans. on Inf. Tech. in Biomedicine*, 8(3):360–376, 2004.

[18] C. Ogilvy, B. Carter, K. S., R. C., and R. Crowell. Temporary vessel occlusion for aneurysm surgery: risk factors for stroke in patients protected by induced hypothermia and hypertension and intravenous mannitol administration. *J. Neurosurg.*, 84(5):785–91, May 1996.

[19] H. M. Pakter, E. Ferlin, S. C. Fuchs, M. K. Maestri, R. S. Moraes, G. Nunes, L. B. Moreira, M. Gus, and F. D. Fuchs. Measuring arteriolar-to-venous ratio in retinal photography of patients with hypertension: Development and application of a new semi-automated method. *Am. J. of Hypertension*, 18(3):417–421, 2004.

[20] N. Patton, T. M. Aslam, T. MacGillivray, I. J. Deary, B. Dhillon, R. H. Eikelboom, K. Yogesan, and I. J. Constable. Retinal image analysis: Concepts, applications and potential. 25:99–127, 2006.

[21] D. Selle, B. Preim, A. Schenk, and H.-O. Peitgen. Analysis of vasculature for liver surgical planning. *IEEE Trans. Med. Imaging.*, 21(11):1344–1357, Nov. 2002.

[22] M. Sofka and C. V. Stewart. Retinal vessel centerline extraction using multiscale matched filters, confidence and edge measures. *IEEE Trans. Med. Imaging.*, 25:1531–1546, 2006.

[23] M. Sonka, A. Stolpen, W. Liang, and R. M. Stefancik. *Handbook of Medical Imaging, Medical Image Processing and Analysis*, volume 2, chapter Vascular Imaging and Analysis., page 809V914. SPIE Press, 2001.

[24] J. Staal, M. Abramoff, M. Niemeijer, M. Viergever, and B. van Ginneken. Ridge based vessel segmentation in color images of the retina. *IEEE Trans. Med. Imaging.*, 23(4):501–509, Apr 2004.

[25] A. Stanton, B. Wasan, A. Cerutti, S. Ford, R. Marsh, P. Sever, S. Thom, and A. Hughes. Vascular network changes in the retina with age and hypertension. *J. of Hypertension*, 13(12):1724–1728, 1995.

[26] T. Wong, L. Hubbard, E. Marino, R. Kronmal, A. Sharrett, D. S. Siscovick, G. Burke, and J. M. Tielsch. "retinal microvascular abnormalities and blood pressure in older people: The cardiovascular health study". *Brit. J. of Ophthal.*, 86(9):1007–1013, 2002.

[27] P. Yim, P. Choyke, and R. Summers. Gray-scale skeletonization of small vessels in magnetic resonance angiography. *IEEE Trans. Med. Imaging.*, 19:568–576, June 2000.